ELSEVIER

Catalysis Today 70 (2001) 411–425

CATALYSIS TODAY

www.elsevier.com/locate/cattod

Nonlinear phenomena during electrochemical oxidation of hydrogen on platinum electrodes☆

Hamilton Varela, Katharina Krischer*,[1]

Fritz-Haber-Institut der Max-Planck-Gesellschaft, Abteilung Physikalische Chemie, Faradayweg 4-6, D-14195 Berlin, Germany

Abstract

H_2 oxidation on Pt electrodes, a comparatively simple electrocatalytic reaction, has been known for a long time to exhibit a variety of complex temporal oscillations, depending on the composition of the supporting electrolyte. We report, on the one hand, recent observations of spatial instabilities in the bistable and oscillatory region in this system. The studies indicate that the spatio-temporal dynamic is by far richer than has been assumed so far. On the other hand, aperiodic responses of the system in cyclic voltammetric experiments are described. This behavior is similar to the one observed in potentiodynamic measurements during the electro-oxidation of small organic molecules. A possible common origin of all these complex, current–voltage responses is discussed.

Keywords: Hydrogen oxidation; Oscillations; Pattern formation; Electrocatalysis

1. Introduction

The electro-oxidation of H_2 is among the most studied electrochemical reactions. This great interest results from fundamental as well as applied aspects. It is apparently one of the simplest electrocatalytic reactions, and thus has served as model system for electrocatalytic oxidation reactions, and it is the anode reaction in the direct H_2/O_2 fuel cell, the most important type of fuel cell [1,2].

The mechanism of electrocatalytic reactions involves the adsorption of an educt or reaction intermediate on the electrode surface. This step causes a strong dependence of the reaction rate not only on the electrode material but also on the composition of the supporting electrolyte since the species dissolved in the electrolyte may also adsorb on the electrode surface. In general, the adsorbed species, often ions, have an inhibitory or accelerating effect on the reaction rate. The repercussion between potential-dependent adsorption of reactants and species of the base electrolyte make the detailed understanding of electrocatalytic reactions a difficult task. Moreover, the different adsorption processes are a source of nonlinear behavior, which further complicates matter [3–5].

H_2 oxidation on Pt electrodes is slowed down by the adsorption of halides, the formation of oxides, and the deposition of various metals on the electrode surface, for example. Thus it is not astonishing that the first observations of periodic variations of the H_2 oxidation current date already back to the first half of the last century [6–8]. In these early works, the oscillatory behavior was shown to be associated with the periodic formation and dissolution of Pt oxides. Horányi and Visy [9] pointed out that Pt oxide must not necessarily

☆ Paper presented at the workshop on "Spatio-temporal catalytic patterns", Haifa, Israel.

* Corresponding author. Tel.: +49-30-8413-5146; fax: +49-30-8413-5106.

E-mail address: krischer@fhi-berlin.mpg.de (K. Krischer).

[1] http://w3.rz-berlin.mpg.de/pc/spatdyn/spatdyn.cgi?home.

0920-5861/01/$ – see front matter
PII: S0920-5861(01)00347-9

participate in an oscillatory cycle during H_2 oxidation. Under galvanostatic conditions they could initiate oscillatory behavior by adding electrosorbing cations to the electrolyte. The oscillating electrode potential remained throughout at potentials negative to the one at which OH adsorption starts. Later it was demonstrated that these oscillations could not be explained by the electrosorption of cations alone. Rather, they result from a competitive adsorption of cations and anions that both reduce the rate of H_2 oxidation [10–12].

The oxidation of H_2 in the presence of electrosorbing cations and anions turned out to exhibit an enormous wealth of complex dynamic behavior, ranging from period doubling cascades, over an interior crisis, which transforms a chaotic attractor with small amplitude oscillations to one with large amplitude bursts, up to intricate sequences of mixed-mode oscillations [13–15].

During the last years, more and more attention has been paid to the spatial extension of the electrode [5,16–54], bringing to light that many nonlinear phenomena encountered in electrochemical systems are accompanied by spatially varying reaction rates.

In the present contribution we compile our recent work on nonlinear phenomena during H_2 oxidation which mainly aimed at an improvement of the current understanding of spatial symmetry breaking in electrochemical systems. We start with the oxidation of H_2 in sulfuric acid, one of the simplest electrocatalytic systems. After a brief description of the voltammetric signature of this system at low electrolyte conductivity, we discuss conditions in which a stable, stationary pattern consisting of two domains with high and low catalytic activity forms. Then, more complex voltammetric behavior is presented, namely aperiodic responses of the current–external voltage (I–U) curve upon periodic cycling of U. The stationary structures as well as the complex series of cyclic voltammograms are associated with oxide formation, and thus should be rather insensitive to the nature of the conducting ions.

In the subsequent examples involving oscillatory instabilities, the presence of cations and anions that competitively adsorb in a certain potential range is essential. Thus, the dynamics depend more sensitively on the composition of the electrolyte. The presented data are from the H_2/Cl^-, Cu^{2+}, H_2SO_4/Pt system. After reviewing the oscillatory mechanism, we demonstrate that both under potentiostatic as well as under galvanostatic conditions the oscillations in the global current or potential, respectively, can be accompanied by wave phenomena.

2. Experimental

The experimental set-up is shown in Fig. 1. A rotating Pt ring (outer diameter 30 mm, width 1 mm) embedded into a Teflon cylinder served as working electrode (WE). Two different configurations were used for the reference electrode (RE). Either a Ag/AgCl electrode (RE1) was put into a J-shaped glass capillary (Haber–Luggin capillary) and the tip of the capillary was located on the axis of the WE at a distance of about 3 mm to the WE, or a Hg/Hg_2SO_4 reference electrode in a separate compartment (RE2) that was connected to the main compartment slightly above the plane of the CE was used. The CE, a 1 mm thick Pt wire bent to a ring of 65 mm in diameter, was located parallel to the WE and at a distance of 45 mm to the WE.

To monitor the angular potential distribution in front of the WE, the tip of a second glass capillary

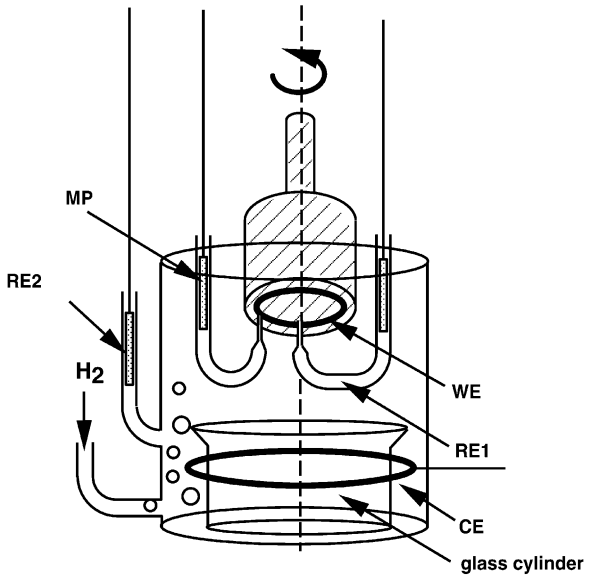

Fig. 1. Scheme of the experimental set-up. WE: working electrode (embedded into a Teflon body), RE: reference electrode (either a Ag/AgCl electrode (RE1) or a Hg/Hg_2SO_4 electrode (RE2)); CE: counter electrode (a Pt ring), MP: potential micro-probe.

equipped with a Ag/AgCl electrode (the potential micro-probe, MP) was placed 1 mm ± 0.2 mm below the Pt ring. During the experiments, the WE was rotated with 20 Hz, and the voltage between MP and WE was measured with an acquisition rate of 1 kHz (i.e. 50 points/rotation), which allowed us to construct a spatio-temporal picture of the potential in front of the WE. As the resistance between MP and WE was negligible, the measured voltage represents the local potential drop across the double layer (called double layer potential, ϕ_{DL}, below) to a good approximation. For further experimental details see Ref. [51].

3. Bistability and stationary domains in the H_2/H_2SO_4/Pt system

3.1. General properties of H_2 oxidation on Pt and experimental results

The electrochemical oxidation of hydrogen on Pt surfaces is known to proceed in three steps [55,56]: (1) the diffusion of H_2 from the bulk electrolyte to the electrode surface, (2) the dissociative adsorption of surface H_2 onto bare Pt sites, and (3) the electrochemical oxidation of adsorbed hydrogen atoms accompanied by hydration:

$$H_2^{bulk} \rightarrow H_2^{surface} \quad (1)$$

$$2Pt + H_2^{surface} \rightarrow 2Pt - H \quad (2)$$

$$Pt - H + H_2O \rightarrow H_3O^+ + e^- + Pt \quad (3)$$

At low overpotentials, the electron transfer step (3) is rate determining, whereas at high potentials mass transfer (1) determines the reaction rate.

If the overpotential exceeds 0.8 V vs. RHE, concomitant to the H_2 oxidation reaction, Pt oxides are formed (steps (4) and (5)).

$$Pt + H_2O \rightarrow Pt - OH + H^+ + e^- \quad (4)$$

$$Pt - OH \rightarrow Pt - O + H^+ + e^- \quad (5)$$

For increasing coverage of chemisorbed oxygen, the hydrogen oxidation current becomes very small because of the negligible dissociation rate of hydrogen (step (2)) on PtO(H).

This set of reactions can be easily observed during potentiodynamic experiments in acidic media [55].

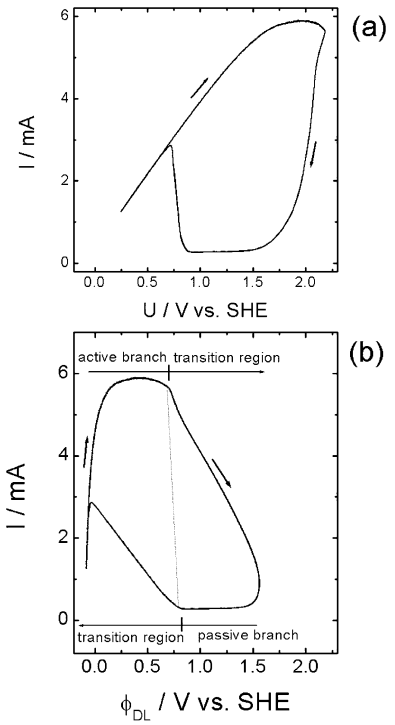

Fig. 2. (a) Cyclic voltammogram of a rotating ring electrode in 1 mM H_2SO_4/H_2 (sat); rotation speed: 20 Hz; scan rate: 100 mV s^{-1}. (b) I–ϕ_{DL} as obtained from (a) by 'IR_Ω correction' according to $U = \phi_{DL} + IR$, where $R = 350\,\Omega$ is the cell resistance.

Fig. 2 shows the cyclic voltammogram of a rotating platinum ring electrode in H_2-saturated, 1 mM sulfuric acid in two representations. In Fig. 2(a), the current, I, is shown as a function of the externally applied potential, U. As a result of the relatively low conductivity of the electrolyte, U deviates considerably from the true electrode potential, ϕ_{DL}. For a given I–U pair ϕ_{DL} is obtained by subtracting the ohmic potential drop through the electrolyte, IR, from U, where R is the cell resistance. The resulting I–ϕ_{DL} curve is shown in Fig. 2(b).

Focussing on Fig. 2(a), the initial linear increase of the current with U when increasing U from the lower turning point reflects the high electrolyte resistance which determines the form of the I–U curve as long as the electron transfer rate (step (3)) controls the current density. The potential-independent current plateau at larger values of U indicates mass transport limitation

(step (1)). Close to the upper turning point, Pt oxide formation sets in (steps (4) and (5)), which leads to a nearly complete inhibition of hydrogen oxidation, as can be seen in the current decrease during the beginning of the negative scan, and to a large hysteresis in the two scan directions. The passive state persists on the reverse scan until the oxide is reduced at about 0.8 V and H_2 is oxidized with the same rate as in the forward scan.

The basic shape of the cyclic voltammogram remains nearly unchanged under stationary conditions, and thus H_2 oxidation on Pt exhibits bistable behavior, the simplest nonlinear phenomenon, in a certain range of the externally applied potential. In the following, we denote the states with high and low current *active* and *passive* states, respectively.

A comparison of Fig. 2(a) and (b) reveals that active and passive branches correspond to different values of the potential drop across the double layer, ϕ_{DL}, and thus, in contrast to the *I–U* curve, the *I*–ϕ_{DL} characteristic is not bistable. The solid curve segments that connect the active and passive branches in Fig. 2(b) result from the transition between the two stable states in Fig. 2(a), and, hence, represent transient behavior. Under stationary conditions *I* is a single-valued function of ϕ_{DL}. The middle branch, which is indicated by the dashed line in Fig. 2(b) possesses a negative differential resistance (NDR) and is unstable under the conditions of the experiment. More generally, it is unstable whenever the cell resistance is larger than $|(Z_F^*)|$, where Z_F^* is the faradaic impedance at the inflection point of the NDR-branch [3]. Then, the system exhibits bistability. In fact, the interaction between an NDR in the *I*–ϕ_{DL} curve and the *IR* drop in the electrolyte is the most common source of bistable behavior in electrochemical systems.

In bistable media, the coexistence of the two stationary states is observed only if the fluctuations present in the system are sufficiently small. Larger perturbations can cause transitions between the two states. In a spatially extended system, the transitions are usually accompanied by propagating waves [57,58]. Recent studies of transitions between active to passive state and vice versa evidenced a sensitive dependence of the front behavior on the position of the reference electrode [51], which had been theoretically predicted [33,59,60].

In the experiments, transitions between the active and passive branches were investigated by pausing a potential sweep on the active branch at a potential close to end of the bistable region. When RE2 was used, i.e. for a large distance between RE and WE, the transitions between the two homogeneous states occurred through nucleation and growth of the globally stable state from the initially metastable one. The transitions from the active to the passive state and vice versa became considerably longer for closer distances between RE and WE [51]. Fig. 3 shows the front behavior found when RE1 was used (i.e. for a distance between WE and RE $\ll$ circumference of WE). For such close distances, the growth of the passive area stopped during the transition, giving rise to stationary potential domains (Fig. 3(b)). In Fig. 3(a), the current transient during the transition is displayed. In the

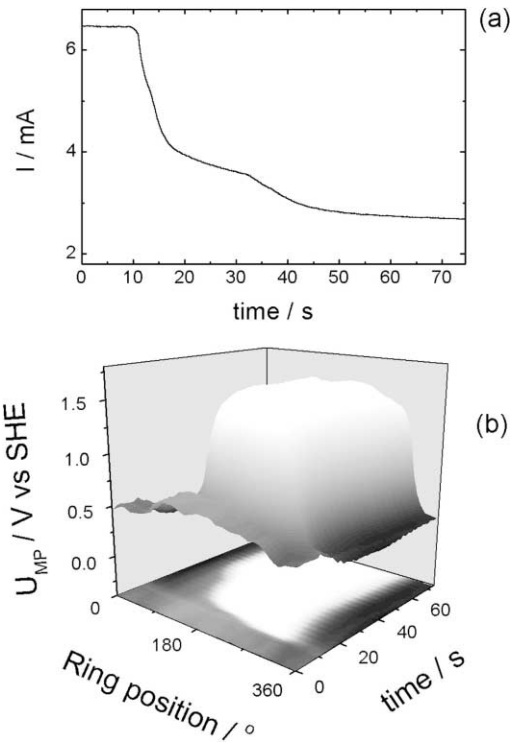

Fig. 3. Stationary structure emerging during an active–passive transition. Distance between the plane of the WE and the tip of the Haber–Luggin capillary (RE1): 3 mm. The external potential (*U*) was fixed at 1.59 V vs. SHE. Cell resistance $R = 176 \pm 10\,\Omega$. (a) Current–time plot. (b) Position–time plots of the local electrode potential.

patterned state, part of the Pt is covered by oxide (white), and thus passive, the other part is a bare Pt surface on which hydrogen oxidation proceeds with a diffusional limited rate (black). The potential difference between the active and the passive domains in Fig. 3(b) amounts to approximately 1.2 V. To get a notion for this value, it should be compared to the theoretical voltage necessary for the decomposition of water into hydrogen and oxygen, which is 1.230 V at 25°C. Thus, in principle, one can imagine that such stationary structures are deliberately produced to run two different reactions in parallel on the electrode.

3.2. Discussion

If the RE is sufficiently far from the WE, the spatial coupling between different positions of the electrode, which is responsible for the expansion of the passive nucleus that emerges due to a fluctuation on the active electrode (i.e. for the motion of the fronts) is due to the electric field in the electrolyte [5,43,44]: The two states possess different potential drops across the double layer, and thus induce an inhomogeneous potential distribution in the electrolyte. The altered potential distribution, in turn, changes the migration currents at the interface. These changes cause a position-dependent recharging of the double layer, which leads to the motion of the interface between the two states. Thus, in electrochemical systems the primary spatial coupling occurs through the electric field, and can be best characterized as migration coupling [49,50].

There is a peculiar difference between this 'electrochemical migration coupling' and the more common diffusion coupling. The range of the coupling, i.e. the range over which the change of a state at a particular location is felt instantaneously, can be tuned by changing the distance between CE and WE. It is long-range for a large distance between WE and CE, whereby large means that the distance between WE and CE is at least as large as the circumference of the WE [43]. For closer distances it becomes progressively more local. For a strongly nonlocal coupling, fronts propagate in an accelerated manner. Such accelerated fronts were first observed for the reduction of persulfate [38]. They were also found during the electro-oxidation reactions of Co [18] and Fe [31], as well as recently in the hydrogen system [51] we consider in this paper.

It had been pointed out that also the distance between WE and RE plays an important role in pattern formation in electrochemical systems [33,46]. The dissipative structure shown in Fig. 3(b) represents a further example of the drastic effect, the position of the RE can have on the dynamics of an electrochemical system. All aspects we discussed in the preceding paragraph about spatial coupling in electrochemical systems neglected the influence of the RE, which is possible as long as the RE is located far away from the working electrode. However, it was shown that for closer distance between WE and RE, the potentiostatic operation mode introduces an additional spatial coupling, namely a negative, global coupling into the system. Global coupling means that a local change of the double layer potential affects the dynamic of the entire electrode instantaneously, or in other words, the local evolution of ϕ_{DL} depends on the spatial mean of ϕ_{DL}, $\langle\phi_{DL}\rangle$. The term negative indicates an antiphase-type behavior that is induced by the global coupling, i.e. at any location the global coupling drives the local value of ϕ_{DL} further away from its mean value $\langle\phi_{DL}\rangle$. Thus, the coupling tends to destabilize homogeneous states. It can lead to the formation of sustained patterns under conditions in which the system is in a state that lies on the NDR branch of the polarization curve. This is true whenever the system is oscillatory or bistable. Thus, stationary domains as in Fig. 3(b) should exist in all systems exhibiting bistability. They are not linked to specific kinetic properties of the H_2 oxidation. Moreover, the formation of stationary domains might also occur when the cell resistance is not large enough to produce bistability and the remaining parameters prevent the occurrence of oscillations. Hence, special care is necessary whenever a Haber–Luggin capillary is used. Considering the fact how widespread the use of a Haber–Luggin capillary is, the 'danger' that it can cause highly nonuniform states cannot be overemphasized.

4. Aperiodic *I–U* response during cyclic voltammetry in the H_2/H_2SO_4/Pt system

4.1. Experimental results

The simple H_2/H_2SO_4/Pt system exhibited another peculiarity arising from the nonlinear properties of the system. During a cyclic voltammetric experiment, the

current–potential (*I–U*) curve usually begins to retrace itself after a finite number of cycles, and in the most common situation the limiting *I–U* curve retraces itself on every cycle, i.e. the *I–U* response has the same period as the periodically cycled external potential. However, under some conditions the interaction between the periodic forcing (or external potential programming) and nonlinearities in the electrochemical process can lead to more complex behavior. The coexistence of more than one *I–U* response during cyclic voltammetric experiments was first observed by Parida and Schell [61] in the electrochemical oxidation of formic acid on a Pt electrode. Subsequently, the same group found this phenomenon during the oxidation of other organic molecules, such as methanol, ethanol, propanol, etc. and discussed it in terms of the reaction between the reaction intermediate PtCO and PtO [62–66]. Cyclic voltammograms with high period and aperiodic responses were also obtained during the anodic dissolution of copper [67]. As observed for the electro-oxidation of organic molecules these authors found the route to chaos through period doubling when one control parameter is changed, such as the upper potential limit.

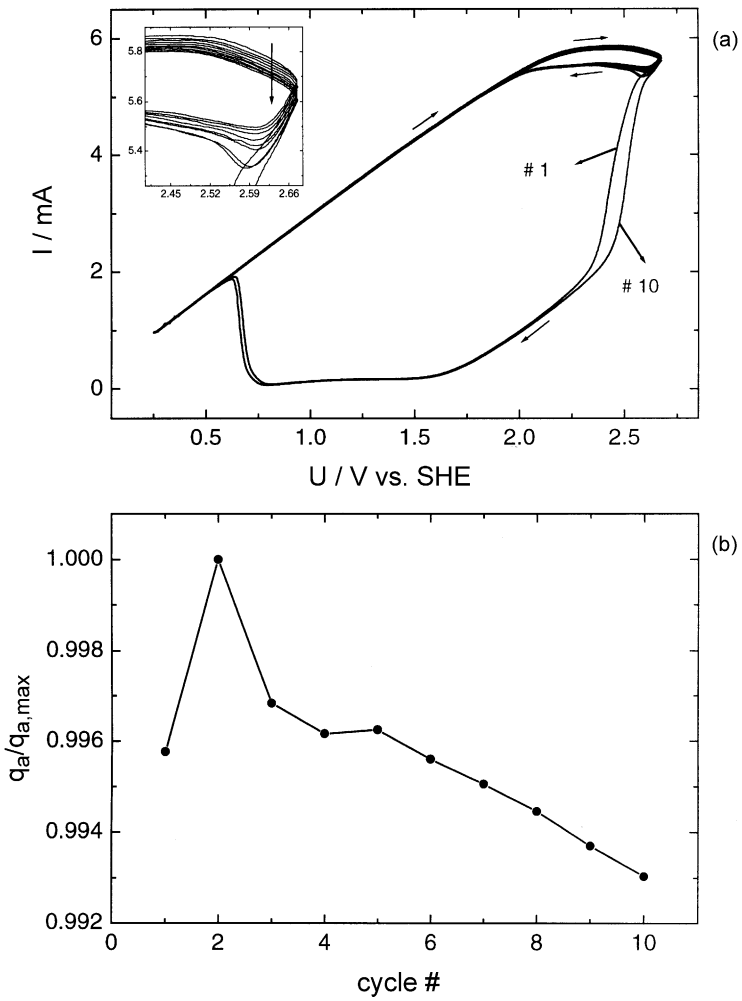

Fig. 4. (a) Sequence of aperiodic *I–U* responses in the course of H_2 electro-oxidation (10 cycles are shown). (b) Plot of the charge that flows during the anodic half cycle of a potential scan, q_a (normalized to the maximum charge obtained, $q_{a,max} = 96.284\,mC$) as a function of the cycle number.

A similar behavior is obtained during H_2 oxidation on Pt. Fig. 4(a) shows part of a sequence of aperiodic *I–U* responses in the course of H_2 electro-oxidation. There are two limiting voltammetric shapes. One of it exhibits a high, mass transport limited current close to the anodic turning point during the positive and negative sweep. The other one involves a transition to small current close to this turning point (c.f. Fig. 2(a)). In Fig. 4, 10 cyclic voltammograms are shown whereby the first (No. 1) and last (No. 10) cycles undergo a transition to the oxide covered surface (an *active/passive* cycle) and the others present a high current in both forward and reverse scans with a slight decrease in current with time (*all-active* cycles). The *I–U* curves close to the upper potential limit are magnified in the inset of Fig. 4(a). In this representation, the activity decrease in consecutive cycles, which is observed in both scan directions, can be seen more clearly. The decrease in the Pt surface activity can be quantified in terms of the charge transferred in the forward scan, since it represents a direct measure of the Pt surface activity towards the H_2 electro-oxidation reaction. A plot of the integrated charge that flows during the positive half cycle (q) as a function of the cycle number is shown in Fig. 4(b). To emphasize this difference in activity, q was normalized to the highest charge obtained, i.e. the charge in the second cyclic voltammogram ($q_{max} = 96.284\,mC$).

The general behavior extracted from these plots is that after an active/passive cycle the electrode reaches its highest activity that decreases in the course of the subsequent cycles until finally another active/passive cycle occurs. The number of cycles between two active/passive cycles, however, seems to be arbitrary. This can be seen in Fig. 5 in which the appearance of the two limiting voltammetric behavior is displayed as a function of the cycle number for 71 cycles. At this point we would like to note that in some experiments we observed for very long cycling times a transition to period 1 behavior with only active/passive cycles. We attribute this change to some superimposed slight parameter shift that is not intrinsically linked to the aperiodic response. We would also like to stress that we have first indications that the temporal behavior during cyclic voltammetry is much richer than discussed here. Though the aperiodic responses exist in large parameter regions, the qualitative behavior can alter with the control parameters, such as the upper turning

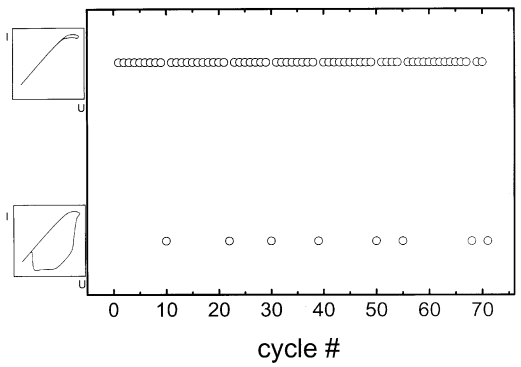

Fig. 5. Type of the limiting voltammetric behavior as a function of the cycle number.

point, and period doubling sequences as observed in other systems [63–67] are likely to exist also during hydrogen oxidation.

4.2. Discussion

From the point of view of electrocatalysis, the most important implication of the presented data is that the reduction of Pt oxide leads to a somewhat more active surface, most likely due to surface roughening. The data suggest that the surface slowly relaxes to its original 'state' with a time constant that is larger than the time of a potential cycle. The aperiodic behavior then seems to be the result of: (a) the interplay between the slow decrease of activity, leading to a more positive double layer potential at the anodic turning point due to the smaller *IR* drop, (b) the period of a voltage cycle, and (c) the nonlinearities present in the current–potential characteristics, most importantly the negative differential resistance (s.a.).

Considering the similar qualitative behavior found in previous works on electro-oxidation of organic molecules on Pt, the complex response of the system to periodic cycling of the potential is very likely to be a general property of electro-oxidation reactions on Pt and other noble metal electrodes. Because the H_2/H_2SO_4/Pt system does not involve any carbon intermediate, this conjecture would imply that the complex dependence of I on U does not require an intermediate that possesses a Pt–C bond, as previously presumed. Rather, it seems to be reasonable that also in the case of the oxidation of small organic

molecules on Pt, the higher periodic or aperiodic CVs arise as a result of the formation and dissolution of Pt oxides only [68].

5. Oscillations and waves in the H_2/Cl^-, Cu^{2+}, H_2SO_4/Pt system

5.1. Oscillatory mechanism and experimental results

Unlike the phenomena discussed so far, the oscillations described in this section are not accompanied by the formation of a passivating oxide layer. Rather, they are linked to a change of the catalytic activity of the Pt electrode as a result of the deposition of Cu and the adsorption of Cl^-. The influence of these adsorbates upon H_2 oxidation on Pt in concentrated H_2SO_4 can be seen in the cyclic voltammograms displayed in Fig. 6. Because of the considerably higher conductivity of the electrolyte compared to the conditions in which the data of Fig. 2 were obtained, the oxidation current in 'pure' H_2SO_4 electrolyte is diffusion limited already at the lower turning point at 100 mV vs. SHE. The positive turning point was chosen slightly negative to the oxide formation such that the diffusion limited value is almost maintained in the whole potential interval of the experiment (short dashed curve in Fig. 6). The addition of Cl^- causes a considerable decrease of the current starting at about 200 mV due to chloride adsorption (dashed curve in Fig. 6). Note that the increasing coverage of Cl^- with positive potentials gives rise to an NDR in the *I–U* curve.

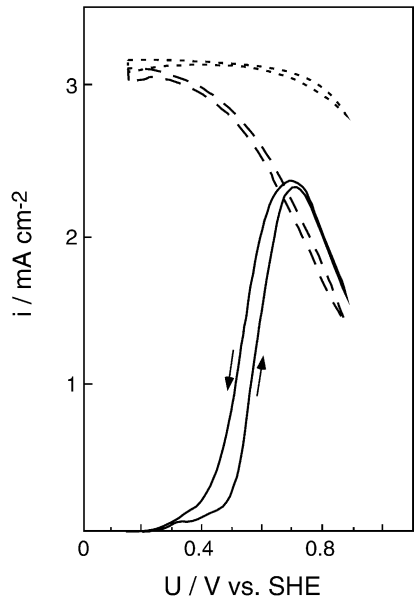

Fig. 6. Cyclic voltammograms of a rotating Pt disk electrode in 0.5 M H_2SO_4, H_2 saturated (short dashed line), 0.5 M H_2SO_4, 10^{-2} M HCl, H_2 saturated (long dashed line), and 0.5 M H_2SO_4, 10^{-2} M HCl, 5×10^{-5} M $CuSO_4$, H_2 saturated (solid line). Electrode area 12.5 mm^2, scan rate of 30 $mV\,s^{-1}$, rotation rate 33 Hz, after [10].

The addition of Cu^{2+} to the Cl^- containing sulfuric acid (solid curve in Fig. 6) inhibits H_2 oxidation at potentials negative to 400 mV almost completely owing to under potential deposition (upd) of 1 monolayer Cu (and at the very negative potentials also Cu bulk deposition). Concurrent with the beginning desorption of the upd monolayer at $U \geq 400$ mV, hydrogen oxidation sets in, and once that the entire Cu is stripped from the electrode, the oxidation current reaches the level of the one in the Cu^{2+}-free, Cl^--containing electrolyte. Owing to the relatively slow Cu-deposition, there is a small, kinetic hysteresis between the forward and the backward scans.

From Fig. 6, it is evident that there is a potential region in which the *I–U* curve possesses an NDR in the Cl^--containing electrolyte that is turned into a positive differential resistance upon addition of Cu^{2+}. Thus, in the presence of Cu^{2+}, the NDR is hidden. Such a hidden NDR leads to oscillatory instabilities in a wide parameter range if the process that causes the NDR (here Cl^- adsorption) is faster than the superimposed process that hides it (in our example Cu deposition). Electrochemical oscillators that are associated with a hidden NDR are commonly abbreviated H-NDR oscillators, or, to further discriminate between an NDR that is part of an *N*-shaped I–ϕ_{DL} curve from one that forms the middle branch of an S-shaped current–potential curve, an HN-NDR oscillator [49,50]. HN-NDR systems oscillate under galvanostatic as well as under potentiostatic conditions [69]. For the latter type of oscillations the cell resistance must be sufficiently large.

A cyclic voltammogram of the H_2/Cl^-, Cu^{2+}, H_2SO_4/Pt system for a much lower conductivity than the one in which the CV of Fig. 6 was obtained is reproduced in Fig. 7(a). The large spike on the reaction controlled branch of the CV points to an oscillatory instability. In fact, when holding *U* constant in a potential interval around the one in which the spike

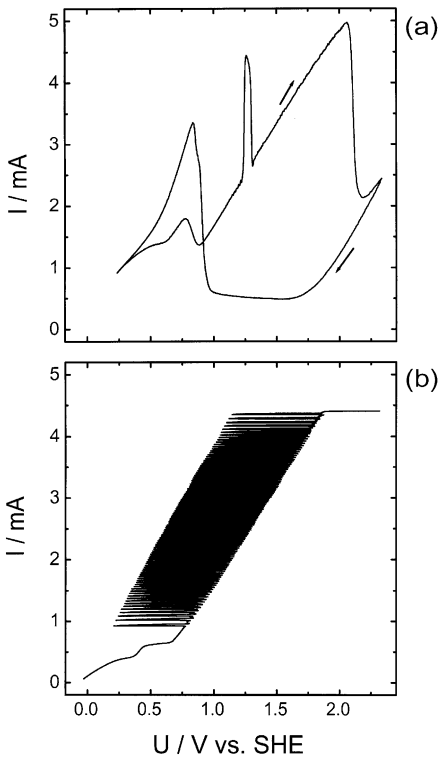

Fig. 7. *I–U* characteristics of the H_2 electro-oxidation reaction on Pt in presence of Cl^- and Cu^{2+}. Electrolyte: 10^{-4} M HCl, 10^{-4} M $CuSO_4$, 10^{-3} M H_2SO_4, H_2 saturated. (a) Potential sweep between 0.235 and 2.335 V, scan rate: 50 mV s^{-1}. (b) Current scan from 0.06 to 4.4 mA, scan rate: 10 μA s^{-1}.

occurs, sustained oscillations are observed. An *I–U* plot of data obtained under galvanostatic conditions is displayed in Fig. 7(b). The oscillatory region covers nearly the entire available current range on the reactive branch.

To obtain a better understanding of the oscillatory instability, it is helpful to develop a qualitative picture of the different stages of an oscillatory cycle under galvanostatic conditions. Model calculations can be found in [11,12]. Starting with a bare Pt electrode, the electrode will take on a low potential value at which H_2 oxidation is reaction controlled. However, at this potential, Cu is also deposited and thus the number of active Pt sites at which H_2 can adsorb are reduced. To keep the current constant on the effectively smaller area, the galvanostat shifts the potential in the positive direction, where two processes occur simultaneously: Cu desorbs and Cl^- adsorbs. Since Cl^- adsorption is faster than Cu desorption, the Pt sites that would become available for H_2 oxidation because of the desorption of Cu are for the most part blocked by Cl^- adsorption. Thus, the potential is driven further into the positive direction where the remaining Cu desorbs more rapidly. This process eventually leads to the situation that more active Pt sites are available than are needed to maintain the set current, and consequently the potential is driven back to more negative values, where the reverse processes happen. The faster rate of Cl^- desorption compared with Cu deposition prevents the system from settling down at a stationary state with an intermediate coverage of Cu and Cl^-, but causes an overshooting of the potential, now to more negative values. A large number of active surface sites become available again for H_2 oxidation, initiating renewed deposition of Cu, and thus a new oscillatory cycle.

Although the temporal instabilities had been known for many years, it was discovered only recently that the homogeneous oscillations are unstable with respect to spatial perturbations for a sufficiently large electrode [51]. In the following, we present further examples of wave phenomena in the oscillatory region of H_2 oxidation. Only the external reference electrode (RE2) was used in order to minimize the additional complication arising from the presence of the negative global coupling when using a Haber–Luggin capillary.

An example for the spatio-temporal dynamics under galvanostatic conditions is displayed in Fig. 8. Fig. 8(a) shows a gray scale representation of the local double layer potential as a function of space (ring-position) and time. In this and the following figures white denotes the highest potential values, black the lowest one. In Fig. 8(a), the data are shown as measured, and at first glance it appears as if the electrode were oscillating homogeneously. However, when inspecting the figure more carefully, a wavy structure is discernible in the transition regions between the black and white ‘sections’. When subtracting the homogeneous oscillation from the spatially resolved data, it becomes evident, that we are dealing with a spatio-temporal phenomenon (Fig. 8(b)). To a first approximation, the inhomogeneously oscillating part can be described by a constant spatial profile similar to a sine wave with wavenumber one whose amplitude oscillates with the period of the homogeneous oscillation. The latter is, up to a constant

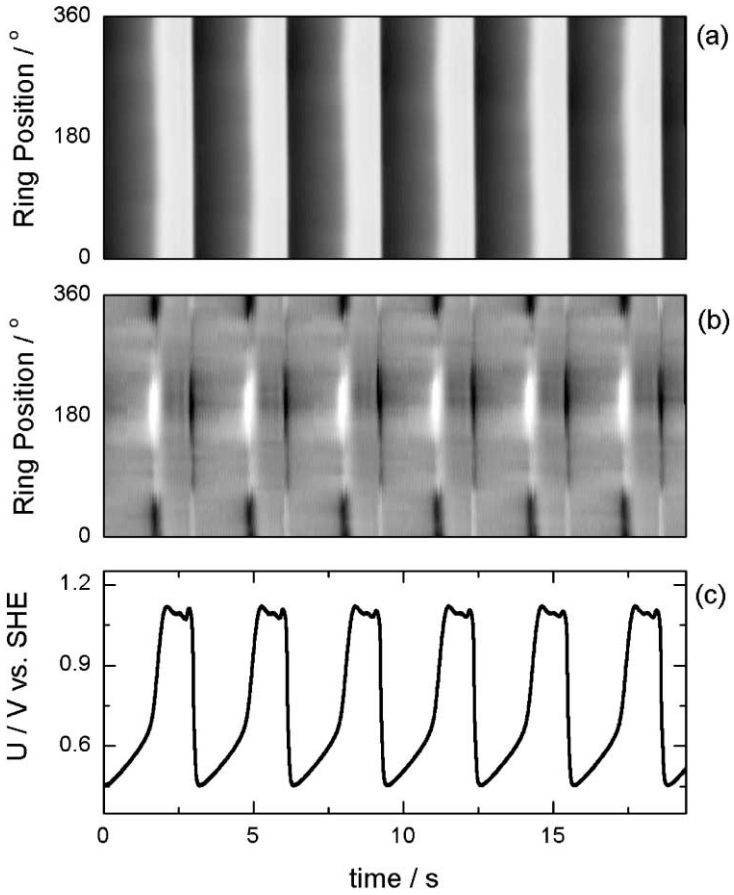

Fig. 8. Position–time plot of the local double layer potential: (a) before and (b) after subtraction of the homogeneously oscillating part during a galvanostatic experiment. (c) Corresponding time series of the global potential. $I = 2\,\text{mA}$; electrolyte: 10^{-3} M H_2SO_4 (H_2 saturated), 10^{-4} M HCl and 10^{-4} M $CuSO_4$; rotation rate 20 Hz. The double layer potential increases from black to white. The grey scales used in (a) and (b) were normalized to the maximum (white) and minimum (black) value of the respective data set displayed.

offset (which results from the *IR* drop in the electrolyte) identical to the measured voltage between WE and RE1 (cf. Fig. 2), and is shown in Fig. 8(c). Both, the homogeneous and inhomogeneous 'modes' exhibit oscillations, whereby the amplitude of the inhomogeneous oscillation (A_1) has bursts to positive values on the rising flank and bursts to negative values on the falling flank of the homogeneous oscillation. In between these outbreaks, A_1 is close to zero. Thus, a time series of A_1 resembles the derivative of the homogeneous oscillation with respect to time, $\mathrm{d}A_0/\mathrm{d}t$, at positions centered around 180°, and it is similar to $-\mathrm{d}A_0/\mathrm{d}t$ at positions around 0° (or 360°).

The spatial structures are more pronounced in the example reproduced in Fig. 9 which was obtained under potentiostatic conditions. Shown are again the spatio-temporal raw data (Fig. 9(a) and (d)), the data obtained after subtraction of the homogeneous oscillations (Fig. 9(b) and (e)) and the time series of the total current (Fig. 9(c) and (f)). Under the experimental conditions, the dynamic exhibited long transients. In the first set (Fig. 9(a)–(c)) a portion of the transient dynamic is shown, whereas the system had settled down to the attractor when the data of Fig. 9(d)–(f) were recorded.

The most striking difference to the data obtained under galvanostatic conditions is that already the raw

data (Fig. 9(a) and (d)) exhibit clearly a spatial symmetry breaking. A comparison of plots in which the inhomogeneous dynamics alone is shown reveals that the dynamics is also qualitatively different. First, on the coarsest level of a description, the electrode can be divided into two parts, one part exhibiting oscillations to larger values of the potential only (i.e. positive amplitude), the other one to smaller values only (negative amplitude). A closer inspection shows that there is a small deflection of the oscillations also to values of the respective reversed sign. However, in contrast to the oscillations shown in Fig. 8, the local reaction rates averaged over time differ considerably such that the symmetry breaking leads to pronounced local differences of the catalytic activity measured over long times.

Second, the inhomogeneous part of the dynamics cannot be described any longer by a single spatial profile which oscillates in amplitude. This can be seen most clearly in Fig. 9(e) in which the 'black', i.e. low potential part seems to emerge at approximately 20° and then to travel along the electrode with increasing amplitude, up to about position 340° where it is extinguished. This indicates that at least two spatial modes are required to describe the overall dynamics.

5.2. Discussion

We have presented only two spatially resolved measurements in the oscillatory regime of H_2 oxidation. However, we found spatially inhomogeneous

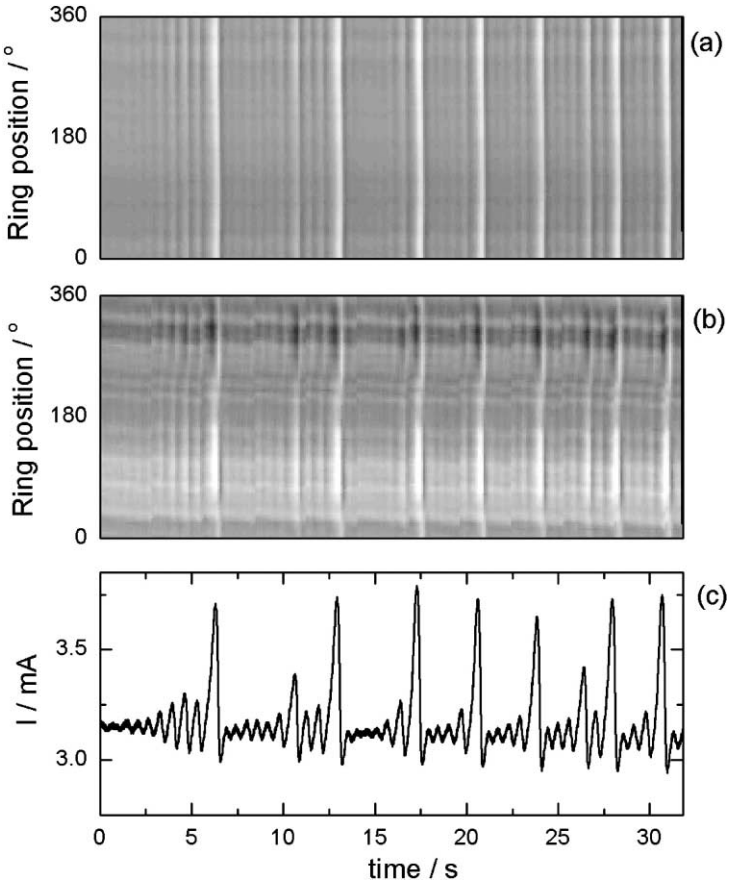

Fig. 9. Position–time plot of the local double layer potential: (a) and (d) before, (b) and (e) after subtraction of the homogeneously oscillating part during a potentiostatic experiment. (c) and (f) corresponding time series of the global current. $U = 1.36$ V; electrolyte: 10^{-3} M H_2SO_4 (H_2 saturated), 10^{-5} M HCl and 10^{-4} M $CuSO_4$; rotation rate 20 Hz. (a)–(c) displays transient behavior, (d)–(f) the long-term dynamic. For the grey scales see caption of Fig. 8.

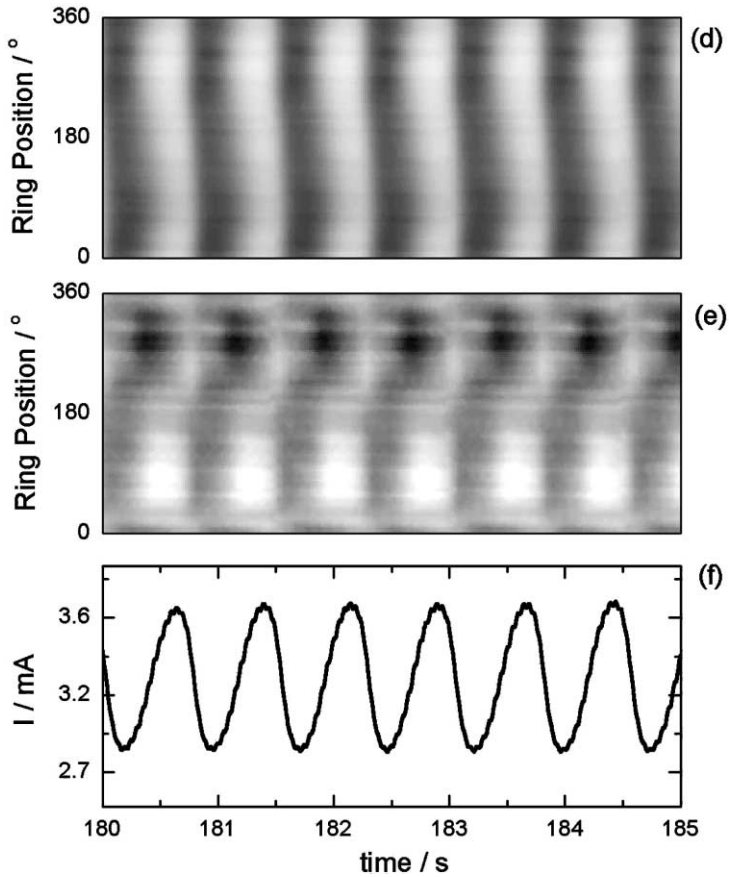

Fig. 9. (*Continued*).

oscillations for all parameters investigated so far (5×10^{-6} M $\leq$ [Cu^{2+}] $\geq 1 \times 10^{-4}$ M; 5×10^{-5} M $\leq$ [Cl^{-}] $\leq 10^{-4}$, 1 mM H_2SO_4), though, for the lowest concentrations used the amplitude of the inhomogeneous structure was substantially smaller than in Fig. 9(b).

Under galvanostatic conditions, the observed behavior was for the most part qualitatively similar to the one displayed in Fig. 8. The oscillations can be described by a superposition of the homogeneous mode and one spatial structure, that were both oscillating with the same period. The maximal amplitude $A_{0,\max}$ of the homogenous oscillation was always considerably larger than the one of the inhomogeneous mode, $A_{1,\max}$. For example, in the data of Fig. 8 $A_{1,\max}/A_{0,\max} = 17\%$. Although we could not observe a transition from a homogeneous to an inhomogeneous oscillation so far, the large amplitude of the homogeneous oscillation suggests that the spatial symmetry breaking results from an instability of the homogeneous *limit cycle* with respect to spatial perturbations. In other words, the local dynamics is oscillatory, and the homogeneous limit cycle is destabilized by the spatial coupling. Theoretically, such type of system is characterized by a negative effective phase diffusion coefficient [70]. From this point of view, we can classify the oscillations in Fig. 8 as being Benjamin–Feir unstable [60] although the dynamics is far from being turbulent.

Benjamin–Feir unstable states were observed in hydrodynamic experiments [71–74]. Concerning reaction–diffusion systems there are hardly any experiments proving the existence of Benjamin–Feir unstable oscillations. The existence of turbulent patterns is reported during CO-oxidation on Pt(110) [75,76]

and the $NO + NH_3$ reaction on Pt(100) [77], however, so far, any analysis of the turbulent state or a discussion of the dynamic regime of the corresponding homogeneous state are missing. In the photosensitive BZ-reaction, oscillatory clusters were observed that can be attributed to a global coupling induced destabilization of the homogeneous limit cycle [78], an effect that has been theoretically predicted in the context of gasphase reactions by Falcke et al. [79]. On a phenomenological level, antiphase oscillations which were observed during the electrodissolution of Ni [80,81] [2] possess a striking similarity to the data presented here. With the information currently available on the bifurcations in this latter system, the question, whether the Ni dissolution was Benjamin–Feir unstable in the above defined sense remains open. Our above considerations suggest that the oscillatory H_2 oxidation in the presence of Cu and Cl^- indeed represents an experimental example for a Benjamin–Feir unstable system. Thus, hydrogen oxidation seems to be a good candidate to narrow the gap in the number of theoretically predicted and experimentally found spatio-temporal bifurcations in systems in which the instabilities result from the interaction of nonlinear local dynamics and a transport process.

When trying to classify the wave patterns observed under potentiostatic conditions (cf. Fig. 9), we met difficulties. As pointed out above, the main characteristic of the pattern was that the inhomogeneous part of the dynamics was oscillating predominantly to positive values of ϕ_{DL} (measured from the mean value) in one-half of the electrode and predominantly to negative values in the other half. In addition, the spatial structures were more pronounced, the ratio of the amplitudes of the homogeneous and inhomogeneous modes amount to $A_{1,max}/A_{0,max} = 41\%$ for Fig. 9(a)–(c) and to $A_{1,max}/A_{0,max} = 51\%$ for Fig. 9(d)–(f). A pronounced antiphase-type behavior with a high percentage of inhomogeneous modes is obtained in the presence of negative global coupling. As was discussed for the H_2/H_2SO_4/Pt system, a negative global coupling is introduced whenever the distance between RE and WE is small. It may destabilize the homogeneous state leading to domain formation (cf. Fig. 3) or a wave bifurcation [35]. While the wave bifurcation gives rise to symmetric behavior and nearly homogeneous reaction rates when averaging in time, one could imagine that an oscillatory instability of a domain structure results in the observed asymmetric oscillations. However, the experiments were carried out with the RE in an external compartment (RE2 in Fig. 1). We cannot exclude that there was a minor negative global coupling left since the junction between the RE compartment and the main cell compartment was slightly above the CE, and hence it was located in a plane parallel to the WE that was not an equipotential plane. However, in the bistable regime of the H_2/H_2SO_4/Pt system we observed always accelerated fronts with this electrode configuration. This is a strong hint that migration coupling dominates the dynamics whereas negative global coupling is minimal, making the domain formation also in the H_2/Cl^-, Cu^{2+}, H_2SO_4/Pt system very unlikely.

In Fig. 9, another difficulty becomes apparent, which is met — to a larger or smaller extent — in all studies of spatio-temporal pattern formation in catalytic systems. The patterns exhibit on top of the 'bipartition' of the electrode a rich fine structure. This fine structure might be an intrinsic feature of the dissipative structure, however, it might also result from an interaction of the nonlinear evolution equations with slight variations of the catalytic activity of the electrode, which are present on any catalytic surface. So far, we were not able to discriminate between these two possibilities. Nevertheless, the data point to the importance of understanding pattern formation in media with distributed parameters. Such studies have just been taken up [82–87]. On the long run, a better understanding of pattern formation on inhomogeneous surfaces might also help designing structured, possibly bimetallic catalysts with qualitatively new properties.

6. Summary

We presented three types of nonlinear behavior during the electrochemical oxidation of H_2 on Pt ring electrodes, a model reaction for the study of complex dynamic behavior in electrocatalytic systems.

In the bistable region of the H_2/H_2SO_4/Pt system stationary inhomogeneous states consisting of two

[2] This interpretation of the Ni data was pointed out to us by J. Christoph.

domains with high and low current density were observed for small distances between RE and WE, i.e. when the IR drop in the electrolyte was minimized by using a Haber–Luggin capillary. The existence of these nonequilibrium structures can be traced back to a negative global coupling through the external control which is operative when the distance between RE and WE is small compared to the distance between RE and CE. This type of spatial symmetry breaking had been found in other experiments [46] as well as in simulations [59,60]. Its occurrence is not linked to the specific electrode kinetics of H_2 oxidation. Rather the use of a Haber–Luggin capillary is likely to destabilize the homogeneous state in the NDR region if the electrode is larger than the minimal size of the domain.

Aperiodic series of cyclic voltammograms were observed when studying the H_2/H_2SO_4/Pt system under potentiodynamic conditions. The complex behavior was shown to be related to the formation and dissolution of Pt oxides during the potential sweep. We suggested that the essential steps causing this complex dynamic are the roughening of the electrode surface, which occurs when the oxide is stripped and leads to a higher catalytic activity, and subsequent surface relaxation during the ongoing cycling. These steps are again independent of the detailed mechanism of H_2 oxidation. It seems to be very likely that they are also the origin for the occurrence of higher periodic or aperiodic cyclic voltammograms that were observed during the oxidation of small organic molecules on Pt and Pd.

The H_2/Cl^-, Cu^{2+}, H_2SO_4/Pt system exhibits temporal oscillations under potentiostatic and under galvanostatic conditions. We found that these temporal oscillations are accompanied by spatial structures in wide parameter ranges. The spatial symmetry breaking occurs most probably from the homogeneous limit cycle. Hence, this would be one of the very rare experimental examples of a Benjamin–Feir unstable system of the reaction-transport type. Under potentiodynamic control more complex spatio-temporal patterns were observed. We could not yet classify these patterns from the point of view of bifurcation analysis. It appears likely, that the spatial fine structure arises as a result of the nontrivial interaction of the nonlinear kinetics and an inhomogeneous parameter distribution, i.e. an inhomogeneous catalytic activity.

Acknowledgements

We are grateful to Peter Grauel for fruitful discussion. KK acknowledges travel support by the Volkswagenstiftung. This work is part of project B4 of the Sfb555, which is supported by the DFG.

References

[1] L. Carrette, K.A. Friedrich, U. Stimming, Chem. Phys. Chem. 1 (2000) 162.
[2] W. Vielstich, Fuel Cells, Wiley/Interscience, New York, 1970.
[3] M.T.M. Koper, Electrochim. Acta 37 (1992) 1771.
[4] M.T.M. Koper, in: I. Prigogine, S.A. Rice (Eds.), Advances in Chemical Physics, Vol. 92, Wiley, New York, 1996, p. 161.
[5] K. Krischer, in: B.E. Conway, J.O.M. Bockris, R. White (Eds.), Modern Aspects of Electrochemistry, Kluwer Academic Publishers/Plenum Press, New York, 1999, p. 1.
[6] M. Thalinger, M. Volmer, Zeit. Phys. Chem. 150 (1930) 401.
[7] G. Armstrong, J.A.V. Butler, Disc. Faraday Soc. 1 (1947) 122.
[8] D.T. Sawyer, E.T. Seo, J. Electroanal. Chem. 5 (1963) 23.
[9] G. Horányi, C. Visy, J. Electroanal. Chem. 103 (1979) 353.
[10] K. Krischer, M. Lübke, W. Wolf, M. Eiswirth, G. Ertl, Electrochim. Acta 40 (1995) 69.
[11] W. Wolf, K. Krischer, M. Lübke, M. Eiswirth, G. Ertl, J. Electroanal. Chem. 385 (1995) 85.
[12] W. Wolf, M. Lübke, M.T.M. Koper, K. Krischer, M. Eiswirth, G. Ertl, J. Electroanal. Chem. 399 (1995) 185.
[13] K. Krischer, M. Lübke, M. Eiswirth, W. Wolf, J.L. Hudson, G. Ertl, Physica D 62 (1993) 123.
[14] K. Krischer, M. Lübke, W. Wolf, M. Eiswirth, G. Ertl, Ber. Bunsenges. Phys. Chem. 95 (1991) 820.
[15] W. Wolf, Ph.D. Thesis, Freie Universität Berlin, Berlin, Germany, 1994.
[16] R.D. Otterstedt, B.J. Green, N.I. Jaeger, P. Plath, M. Pritzker, J.L. Hudson, Electrochem. Soc. Proc. 98 (10) (1998) 178.
[17] R.D. Otterstedt, P.J. Plath, N.I. Jaeger, J.L. Hudson, Phys. Rev. E 54 (1996) 3744.
[18] R.D. Otterstedt, P.J. Plath, N.I. Jaeger, J.C. Sayer, J.L. Hudson, Chem. Eng. Sci. 51 (1996) 1747.
[19] R.D. Otterstedt, N.I. Jaeger, P.J. Plath, Int. J. Bifurc. Chaos 4 (1994) 1265.
[20] R.D. Otterstedt, N.I. Jaeger, P.J. Plath, J.L. Hudson, Phys. Rev. E 58 (1998) 6810.
[21] R.D. Otterstedt, N.I. Jaeger, P.J. Plath, J.L. Hudson, Chem. Eng. Sci. 54 (1999) 1221.
[22] R.D. Otterstedt, P.J. Plath, N.I. Jaeger, J.L. Hudson, J. Chem. Soc., Faraday Trans. 92 (1996) 2933.
[23] J.L. Hudson, J. Tabora, K. Krischer, I.G. Kevrekidis, Phys. Lett. A 179 (1993) 355.
[24] J.C. Sayer, J.L. Hudson, I&EC Res. 34 (1995) 3246.
[25] Z. Fei, R.G. Kelly, J.L. Hudson, J. Phys. Chem. 100 (1996) 18986.
[26] I.Z. Kiss, W. Wang, J.L. Hudson, J. Phys. Chem. B 103 (1999) 11433.

[27] I.Z. Kiss, W. Wang, J.L. Hudson, Phys. Chem. Chem. Phys. 2 (2000) 3847.
[28] I.Z. Kiss, V. Gaspar, J.L. Hudson, J. Phys. Chem. B 104 (2000) 7554.
[29] W. Wang, I.Z. Kiss, J.L. Hudson, Chaos 10 (2000) 248.
[30] S. Nakabayashi, R. Baba, Y. Shiomi, Chem. Phys. Lett. 287 (1998) 632.
[31] R. Baba, Y. Shiomi, S. Nakabayashi, Chem. Eng. Sci. 55 (2000) 217.
[32] A. Karantoni, S. Nakabayashi, Electrochim. Acta 46 (2000) 745.
[33] J. Christoph, R.D. Otterstedt, M. Eiswirth, N.I. Jaeger, J.L. Hudson, J. Chem. Phys. 110 (1999) 8614.
[34] J. Christoph, P. Strasser, M. Eiswirth, G. Ertl, Science 284 (1999) 291.
[35] P. Strasser, J. Christoph, W.-F. Lin, M. Eiswirth, J.L. Hudson, J. Phys. Chem. B 104 (2000) 1854.
[36] J. Lee, J. Christoph, P. Strasser, M. Eiswirth, G. Ertl, J. Chem. Phys. 115 (2001) 1485.
[37] Y.-J. Li, J. Oslonovitch, N. Mazouz, F. Plenge, K. Krischer, G. Ertl, Science 291 (2001) 2395.
[38] G. Flätgen, K. Krischer, Phys. Rev. E 51 (1995) 3997.
[39] G. Flätgen, K. Krischer, B. Pettinger, K. Doblhofer, H. Junkes, G. Ertl, Science 269 (1995) 668.
[40] G. Flätgen, K. Krischer, G. Ertl, Z. Naturforsch. 50a (1995) 1097.
[41] G. Flätgen, K. Krischer, J. Chem. Phys. 103 (1995) 5428.
[42] G. Flätgen, K. Krischer, G. Ertl, J. Electroanal. Chem. 409 (1996) 183.
[43] N. Mazouz, G. Flätgen, K. Krischer, Phys. Rev. E 55 (1997) 2260.
[44] N. Mazouz, K. Krischer, G. Flätgen, G. Ertl, J. Phys. Chem. 101 (1997) 2403.
[45] N. Mazouz, G. Flätgen, K. Krischer, I.G. Kevrekidis, J. Electrochem. Soc. 145 (1998) 2404.
[46] P. Grauel, J. Christoph, G. Flätgen, K. Krischer, J. Phys. Chem. B 102 (1998) 10264.
[47] N. Mazouz, K. Krischer, J. Phys. Chem. B 104 (2000) 6081.
[48] K. Krischer, N. Mazouz, G. Flätgen, J. Phys. Chem. 104 (2000) 7545.
[49] K. Krischer, N. Mazouz, P. Grauel, Angew. Chem. Int. Edit. 40 (2001) 851.
[50] K. Krischer, J. Electroanal. Chem. 501 (2001) 1.
[51] P. Grauel, K. Krischer, Phys. Chem. Chem. Phys. 3 (2001) 2497.
[52] K. Agladze, O. Steinbock, J. Phys. Chem. A 104 (2000) 9816.
[53] S. Bandyopadhyay, A.E. Miller, H.-C. Chang, G. Banerjee, V. Yuzhakov, D.F. Yue, R.E. Ricker, J. Jones, J.A. Eastman, E. Baugher, M. Chandrasekhar, Nanotechnology 7 (1996) 360.
[54] V.V. Yuzhakov, P.V. Takhistov, A.E. Miller, H.-C. Chang, Chaos 9 (1999) 62.
[55] C.H. Hamann, A. Hamnett, W. Vielstich, Electrochemistry, Wiley/VCH, Weinheim, 1998.
[56] W. Schmickler, Interfacial Electrochemistry, Oxford University Press, New York, 1996.
[57] A.S. Mikhailov, Foundations of Synergetics I, Springer, Berlin, 1994.
[58] J.D. Murray, Mathematical Biology, Springer, Berlin, 1990.
[59] A. Birzu, B.J. Green, R.D. Otterstedt, N.I. Jaeger, J.L. Hudson, Phys. Chem. Chem. Phys. 2 (2000) 2715.
[60] J. Christoph, Ph.D. Thesis, Freie Universität Berlin, Berlin, Germany, 1999.
[61] G.R. Parida, M. Schell, J. Phys. Chem. 95 (1991) 2356.
[62] M. Schell, X.R. Cai, J. Chem. Soc., Faraday Trans. 87 (1991) 2255.
[63] M. Schell, X.R. Cai, Electrochim. Acta 38 (1993) 519.
[64] Y.H. Xu, A. Amini, M. Schell, J. Phys. Chem. 98 (1994) 12759.
[65] Y.H. Xu, A. Amini, M. Schell, J. Electroanal. Chem. 398 (1995) 95.
[66] Z. Zdraveski, Y.H. Xu, A. Amini, M. Schell, J. Chem. Soc., Faraday Trans. 92 (1996) 395.
[67] M. Dolata, A.L. Kawczynski, Pol. J. Chem. 72 (2000) 1625.
[68] H. Varela, K. Krischer, Unpublished results.
[69] M.T.M. Koper, J. Electroanal. Chem. 409 (1996) 175.
[70] Y. Kuramoto, Chemical Oscillations, Waves and Turbulence, Springer, Berlin, 1984.
[71] T. Benjamin, J. Feir, J. Fluid Mech. 27 (1967) 417.
[72] W.K. Melville, J. Fluid Mech. 115 (1982) 165.
[73] B.M. Lake, H.C. Yuen, J. Fluid Mech. 88 (1977) 75.
[74] Y. Liu, R.E. Ecke, Phys. Rev. Lett. 78 (1997) 4391.
[75] S. Jakubith, H.H. Rotermund, W. Engel, A.v. Oertzen, G. Ertl, Phys. Rev. Lett. 65 (1990) 3013.
[76] M. Kim, M. Bertram, M. Pollmann, A.V. Oertzen, A.S. Mikhailov, H.H. Rotermund, G. Ertl, Science 292 (2001) 1357.
[77] G. Veser, F. Esch, R. Imbihl, Catal. Lett. 13 (1992) 371.
[78] V.K. Vanag, L. Yang, M. Dolnik, A.M. Zhabotinskz, I.R. Epstein, Nature 406 (2000) 389.
[79] M. Falcke, H. Engel, M. Neufeld, Phys. Rev. E 52 (1995) 763.
[80] O. Lev, M. Sheintuch, L.M. Pismen, C. Yarnitzky, Nature 336 (1988) 488.
[81] O. Lev, M. Sheintuch, H. Yarnitsky, L.M. Pismen, Chem. Eng. Sci. 45 (1990) 839.
[82] M.A. Liauw, J. Ning, D. Luss, J. Chem. Phys. 104 (1996) 5657.
[83] M. Pollmann, H.H. Rotermund, G. Ertl, X. Li, I.G. Kevrekidis, Phys. Rev. Lett. 86 (2001) 6038.
[84] S.Y. Shvartsman, E. Schütz, R. Imbihl, I.G. Kevrekidis, Phys. Rev. Lett. 83 (1999) 2857.
[85] M.D. Graham, I.G. Kevrekidis, K. Asakura, J. Lauterbach, K. Krischer, H.H. Rotermund, G. Ertl, Science 270 (1994) 608.
[86] M. Bär, I.G. Kevrekidis, H.H. Rotermund, G. Ertl, Phys. Rev. E 52 (1995) R5739.
[87] I. Schebesch, H. Engel, Phys. Rev. E 57 (1998) 3905.